Available online at www.sciencedirect.com

SCIENCE DIRECT®

Earth and Planetary Science Letters 224 (2004) 461–475

EPSL

www.elsevier.com/locate/epsl

Effects of nanoscale exsolution in hematite–ilmenite on the acquisition of stable natural remanent magnetization

Takeshi Kasama[a,*], Suzanne A. McEnroe[b], Noriaki Ozaki[c], Toshihiro Kogure[d], Andrew Putnis[a]

[a] *Institut für Mineralogie, Universität Münster, Corrensstrasse 24, D-48149 Münster, Germany*
[b] *Geological Survey of Norway, N-7491 Trondheim, Norway*
[c] *CREST, Japan Science and Technology Corporation, Honcho 4-1-8, Kawaguchi, Saitama 332-0012, Japan*
[d] *Department of Earth and Planetary Science, The University of Tokyo, Hongo 7-3-1, Tokyo 113-0033, Japan*

Received 4 October 2003; received in revised form 25 November 2003; accepted 17 May 2004

Abstract

To investigate the acquisition mechanism of high and stable natural remanent magnetization (NRM) in rocks of the Russell Belt, Adirondack Mountains, New York, we examined the exsolution microstructures and compositions of magnetic minerals using three samples with different magnetic properties. The samples contain titanohematite with ilmenite lamellae, end-member hematite without lamellae and rare magnetite as potential carriers for the NRM. Transmission electron microscopy (TEM) observations and element mapping by energy-filtered TEM (EFTEM) of the titanohematite indicated that very fine ilmenite lamellae with a minimum thickness ~ 2 nm are abundant between larger ilmenite lamellae a few hundreds of nanometers thick. The ilmenite lamellae and titanohematite hosts, with the compositions of $Ilm_{90-100}Hem_{10-0}$ and $Ilm_{7-16}Hem_{93-84}$, respectively, share (001) planes, and the abundant fine ilmenite lamellae have coherent, sharp structural and compositional interfaces with their titanohematite hosts. Comparison between samples shows that the magnetization is correlated with the amount of fine exsolution lamellae. These results are consistent with the lamellar magnetism hypothesis, suggesting that the acquisition of high and stable NRM is related to the interfacial area between fine ilmenite lamellae and their host titanohematite. End-member hematite with a multi-domain magnetic structure only contributes a minor amount to the NRM in these samples.

Keywords: hematite; ilmenite; titanohematite; magnetite; nanoscale exsolution lamellae; magnetism; TEM

1. Introduction

The magnetic signal of rocks arises mainly from minerals of the magnetite–ulvöspinel and hematite–ilmenite solid solutions, and iron sulfides, which are abundant in a wide range of rocks in the Earth's crust [1–3]. In particular, magnetite is the most common phase to dominate the magnetization induced by the present geomagnetic field. On the other hand, magnetite–ulvöspinel solid solutions, hematite–ilmenite solid solutions and iron sulfides are known well as potential minerals contributing to natural remanent magnetization (NRM) in rocks. Since the early studies

* Corresponding author. Present address: Department of Materials Science and Metallurgy, University of Cambridge, Pembroke Street, Cambridge CB2 3QZ, United Kingdom. Tel.: +44-1223-334597; fax: +44-1223-334563.
E-mail address: tk305@cam.ac.uk (T. Kasama).

0012-821X/$ - see front matter © 2004 Elsevier B.V. All rights reserved.
doi:10.1016/j.epsl.2004.05.027

of rock magnetism, the relationships between magnetic properties and microstructure in minerals responsible for the magnetic record have been an elusive topic [4,5]. Magnetite–ulvöspinel solid solutions are the most strongly magnetic minerals in rocks. At small grain sizes (0.02 to a few micrometers), they have single-domain (SD) to pseudo-single-domain (PSD) magnetic structures and can be dominant carriers for NRM [6].

Hematite–ilmenite solid solutions in the composition range $Ilm_{50-80}Hem_{50-20}$ have a Ti-ordered $R\bar{3}$ structure with strong ferrimagnetism at low temperature. However, except when rapidly cooled from high temperature, such compositions would be destroyed by exsolution and would be unlikely to contribute substantially to NRM in crustal rocks [2,7,8]. Rapidly cooled hematite–ilmenite solid solution with these compositions also has the ability to acquire self-reversed thermal remanent magnetization (TRM) [2,9]. The acquisition mechanism of self-reversed TRM is basically explained by magnetic coupling between two neighboring different phases with respect to structure, chemistry and magnetic properties, although several models for the mechanism have been proposed [10].

Early experimental works by Syono et al. [11] and Uyeda [12] have shown that multidomain (MD) size grains of hematite carry a large TRM. Clark [13] plotted experimental data on SD and MD size hematite and showed the very large range of TRMs that can occur due to the different domain structures and blocking temperatures. Dunlop and Kletetschka [14] have suggested that MD size hematite with sizes 20–200 μm can acquire strong TRM because it is nearly saturated with remanent magnetization by a weak magnetic field.

Numerous authors have discussed the oxide mineralogy and petrology of ilmeno-hematite (i.e., hematite with ilmenite lamellae) and hemo-ilmenite (i.e., ilmenite with hematite lamellae) with respect to their contribution to crustal magnetization and magnetic anomalies [15–24]. In this paper, ''lamellae'' are used to denote lens- and plate-like precipitates that are formed within their host by exsolution and are crystallographically coherent or semi-coherent with their host. The recent studies on both igneous and metamorphic rocks that contain oxides with nanometer scale exsolution lamellae of hematite and ilmenite, whose chemical compositions are entirely different from those of the intermediate hematite–ilmenite solid solutions, have been shown to be very magnetic. These rocks all have a strong NRM that dominates the magnetic response of rock bodies. Monte Carlo simulations have suggested that a ferrimagnetic moment of an intergrowth of hematite and ilmenite could be due to the arrangement of cations and spins at the interfaces between hematite and ilmenite, a phenomenon defined as ''lamellar magnetism'' [25–27]. The ferrimagnetic moment occurs in one octahedral layer (~ 0.23 nm) of the interface between hematite and ilmenite, and the cation layer in the octahedral layer does not correspond to the chemistry of either hematite or ilmenite. Robinson et al. [26] calculated that the saturation magnetization of an intergrowth of hematite and ilmenite lamellae can be 22 times stronger than that of end-member hematite.

McEnroe et al. [24] carried out experiments on nearly a pure hemo-ilmenite rock with high and stable NRM, and concluded that the presence of a fine microstructure of hematite and ilmenite lamellae may account for the NRM because the magnetization in these samples was too high to be solely due to the spin-canted antiferromagnetic moment of hematite and the blocking temperatures were above that of magnetite. Although their results supported the lamellar magnetism hypothesis, only a few cases of magnetic acquisition in nature have been attributed to the presence lamellar intergrowths [23,24]. These studies concluded that the cause of the high NRM is ''lamellar magnetism''.

McEnroe and Brown [21] examined constituent minerals and magnetic properties of the metamorphic rocks in a region with a remanent-controlled aeromagnetic anomaly in the Russell Belt, northwest Adirondack Mountains, New York. They found millimeter size grains of titanohematite with abundant ilmenite, pyrophanite [$MnTiO_3$], spinel [$MgAl_2O_4$] and corundum [Al_2O_3] lamellae and concluded that these grains behaved as an array of small SD grains because of the abundant microstructures and defects caused by the exsolution lamellae. Merrill [28] attributed high coercivities of exsolved minerals in the hematite–ilmenite series to magnetostrictive effects associated with exsolution. However, the effects of chemical composition and microstructure of titanohematite on the intensity

Table 1
Magnetic properties of the sample used in the present study

Sample	SUSC[a] (SI)	NRM[a] (A/m)	I[a] (°)	D[a] (°)	M_s (mAm^2/kg)	M_{rs} (mAm^2/kg)	M_{rs}/M_s
AD34-5	3.27×10^{-4}	8.453	−61.5	263.4	311	207	0.67
AD34-4B	6.97×10^{-3}	7.096	−63.3	268.3	250	162	0.65
RS6-2-1	3.72×10^{-4}	0.145	−43.1	285.7	37	23	0.62

SUSC, susceptibility; NRM, natural remanent magnetization; I, inclination; D, declination; M_s, saturation magnetization; M_{rs}, saturation remanence; M_{rs}/M_s, ratio of saturation remanence to saturation magnetization [21].

and stability of the NRM were not conclusively demonstrated.

We chose three samples from the collection studied by McEnroe and Brown [21] in order to investigate the acquisition mechanism of high and stable NRM in the Russell Belt gneiss samples. One has very low susceptibility and high NRM (AD34-5), the second has higher susceptibility and high NRM (AD34-4B) and the third has very low susceptibility and low NRM (RS6-2-1) (Table 1). Koenigsberger ratios (Q-values), calculated by dividing NRM by induced magnetization (=susceptibility × ambient magnetic field), range from 9 to 562, indicating that the remanences in these samples will dominate the magnetic response. Sample AD34-5 has the highest Q-value and AD6-2-1 the lowest. Because these samples are all from the same location and have experienced the same metamorphic conditions, the large variations in magnetic properties make them ideal for examining relationships between microstructures and magnetic properties. We studied the microstructures and compositions of the magnetic minerals by mainly light microscopy (LM), scanning electron microscopy (SEM) and transmission electron microscopy (TEM).

2. Samples

Metamorphic rock samples are from the Russell Belt, northwest Adirondack Mountains, New York. The geological setting and the constituent minerals, chemistry and magnetic properties of the samples are discussed in detail by McEnroe and Brown [21] who gave the following description: The sillimanite–microcline gneisses are interpreted to have been felsic volcanic rocks hydrothermally altered in their primary environment, then metamorphosed to granulite grade. Table 2 shows the magnetic minerals observed in the Russell Belt samples by this study and McEnroe and Brown [21] and gives their known magnetic properties. The magnetic properties suggest magnetite, maghemite, hematite and titanohematite as potential NRM carriers. The other minerals were microcline, sillimanite, quartz, plagioclase, muscovite and biotite.

The three rock samples used in this study, AD34-4B, AD34-5 and RS6-2-1, are similar except that RS6-2-1 has more quartz and sericitized plagioclase, and a smaller quantity of microcline, muscovite and sillimanite. Chlorite replacing biotite and veins of chlorite in all the samples indicated the evidence of local late alteration. This mineralogy is consistent with the description by Buddington et al. [30], who indicated the presence of late stage hydrothermal

Table 2
Magnetic minerals present in the Russell Belt samples and their magnetic properties

Mineral	Formula	Magnetic order[a]	T_C or T_N[b] (°C)	Reference
Magnetite[c]	Fe_3O_4	FM	580	[6]
Maghemite	γ-Fe_2O_3	FM	590–675	[6]
Hematite[c]	α-Fe_2O_3	CAF	675	[6]
Titanohematite[c]	$xFe_2O_3\cdot(1-x)FeTiO_3$ ($x=0.83$)[d]	CAF	520[e]	[23]
Ilmenite[c]	$FeTiO_3$	PM	−213	[24]
Pyrophanite[c]	$MnTiO_3$	PM	−210	[29]

FM, ferrimagnetism; CAF, canted-antiferromagnetism; PM, paramagnetism.

[a] At room temperature.

[b] T_C and T_N are Curie and Néel temperatures, respectively.

[c] Minerals that have already been reported by McEnroe and Brown [21].

[d] Typical composition of titanohematite grains in the Russell Belt samples analyzed by EPMA [21].

[e] Predicted T_N based on a CAF titanohematite.

alteration in this area. The magnetic properties of these samples are given in Table 1.

3. Analytical methods

Micro-scale observations of the distribution of opaque minerals and their identification were performed by LM and field-emission SEM (JEOL JEM6300F) with an energy dispersive X-ray spectrometer (EDX) and back-scatter detector. The volume percentages of the opaque minerals were determined by counting the opaque minerals in thin sections and calculated as an average of three thin sections per each sample. For SEM, thin sections were highly polished and coated with C. Major constituent minerals of the rock samples were also examined by X-ray powder diffraction (XRD) analysis. XRD patterns were obtained by X-ray diffractometry (Philips X'Pert) using monochromatized CuKα radiation at 45 kV and 40 mA.

Phase identification and crystallographic orientation of the phases within the opaque mineral grains were also studied by electron back-scattered diffraction (EBSD), whose pattern is a Kikuchi pattern formed by back-scattered electrons on a phosphor screen distant from the specimen and can provide crystallographic information from SEM with spatial resolution of <1 μm. They were collected using a ThermoNoran Phase ID system attached to a Hitachi S4500 field-emission SEM operating at 20 kV. For EBSD, thin sections of rock samples were further polished using colloidal silica and lightly coated with C. For TEM, $\sim$30-μm-thick slices were removed from thin sections polished mechanically and thinned to electron transparency by Ar ion milling. The thinned specimens were coated with C before they were observed by TEM.

Observations of the microstructure in Fe- and/or Ti-bearing oxide minerals were carried out by conventional TEM, high-resolution TEM (HRTEM) and energy-filtered TEM (EFTEM). The TEM observations were performed at 300 kV using a JEOL JEM3010. Element maps by EFTEM were obtained by a Gatan Imaging Filter, which is operated by Gatan EL/P program packages. To calculate the element maps, the three-window method was used for the background correction. A detailed description of the method is given in Golla and Putnis [31]. A quantitative element analysis was made by EDX attached to TEM with Oxford Link Isis 300 software. We used a spot size of 3 nm, count time of 90 s and a specimen of $\sim$100 nm in thickness. The element concentrations were calculated using theoretical *k*-factors given by the manufacturer and corrected for thickness. Golla and Putnis [31] have shown that the *k*-factors given by the manufacturer for the used TEM are in good agreement with those obtained experimentally.

Measurements of the magnetic susceptibility as a function of temperature were made in air using an AGICO KLY3-CS3/CSL susceptibility bridge operating at a field of 300 A/m. Measurements of susceptibility were made from room temperature to 700 °C and back to room temperature at a rate of 11 °C/min. Low temperature susceptibility measurements were made by naturally warming the sample to room temperature after first cooling it to liquid nitrogen temperature (-196 °C). Susceptibility data were corrected for the diamagnetic susceptibility of the empty furnace assembly and then calculated to the mass susceptibility. Room temperature hysteresis properties were measured on a vibrating sample magnetometer (Princeton Applied Research) in a maximum field of 1 T at ETH and carried out using three specimen chips per each sample.

4. Results

4.1. Opaque minerals in rock samples

Opaque minerals in AD34-5 and AD34-4B made up $\sim$5% of the rock and those in the RS6-2-1 only $\sim$2% of the rock (Table 3). Optically opaque minerals can be classified mainly into two different types: titanohematite with exsolution lamellae, and hematite without lamellae. In the former, the grains, hereafter referred to as ''titanohematite with lamellae'', contained ilmenite, rutile, pyrophanite and spinel as exsolution lamellae, and make up 4.8%, 4.1% and 1.0% of AD34-5, AD34-4B and RS6-2-1, respectively. Hematite without lamellae, hereafter referred to as ''end-member hematite'', which was formed by replacing magnetite (i.e., martization), was revealed to be the end-member composition or that close to the end-member by SEM–EDX and TEM–EDX. The

Table 3
Volume ratios of opaque minerals, titanohematite with lamellae and end-member hematite in the whole samples and grain sizes of titanohematite with lamellae and end-member hematite

Sample	Volume ratio (%)[a]			Grain size (μm)[b]	
	Opaque minerals[c]	Titanohematite with lamellae	End-member hematite	Titanohematite with lamellae	End-member hematite[d]
AD34-5	5.2	4.8	0.4	240 (50–800)	130 (<350)
AD34-4B	5.0	4.1	0.9	220 (40–650)	170 (<500)
RS6-2-1	1.8	1.0	0.8	110 (25–400)	110 (<250)

[a] Volume percentages were determined by counting on the thin sections using transmitted or reflected LMs (transmitted LM only gives total opaques).
[b] Values without parentheses were averages of >50 grain sizes measured, and ones with parentheses a range of the measured grain sizes.
[c] Magnetite coexisting with end-member hematite made up less than 0.1% of the rocks in all three samples.
[d] The grain size of end-member hematite means the size regarded as a single-crystal under LM.

end-member hematite grains were mostly 50–500 μm in size and made up 0.4%, 0.9% and 0.8% of each sample of AD34-5, AD34-4B and RS6-2-1 but locally contained magnetite. The volume ratios of titanohematite with lamellae and end-member hematite as well as their grain sizes, which were directly examined from thin sections by using LM, are shown in Table 3.

Although AD34-5 and AD34-4B are similar to one another with respect to the total amount of opaque minerals, AD34-4B has significantly more and larger end-member hematite grains than AD34-5 in which the opaque minerals are mostly titanohematite with lamellae. In RS6-2-1, the amount of titanohematite with lamellae is only 20–25% of that in the other two samples and with half the grain size. Magnetite made up less than 0.1% of the rocks in the three samples and in particular magnetite in AD34-5 and RS6-2-1 was very rare. As minor opaque minerals, ilmenite in chlorite, hematite with rutile along titanohematite grain boundaries and secondary vein-like hematite were also observed in all the samples.

4.2. SEM observations of titanohematite grains with lamellae

Titanohematite grains imaged by SEM in AD34-5 contain ilmenite and rutile lamellae, which have various shapes, and also locally spinel (Table 4). The parts containing ilmenite and plate-like rutile lamellae are usually separated from one another within titanohematite grains (Fig. 1a), with far more areas containing ilmenite than rutile. The ilmenite lamellae are mostly lens- and cylinder-like shapes (Fig. 1b and c). Rutile lamellae with lengths >1 μm usually have rough and complex surfaces (Fig. 1b and

Table 4
Features of major lamellae in the titanohematite grains observed by SEM and TEM

Sample	Lamella	Shape	Thickness	Figure number
AD34-5, AD34-4B	Ilmenite[a]	Lens-like	~ 2 nm to 1 μm	1c, 1d, 2a, 2b[b], 2d[b], 2e, 2i[b]
		Cylinder-like	0.1–1 μm	1b, 2a, 2c
	Rutile[c]	Plate-like	1–2 μm	1a
		Rough, complex	0.2–1 μm	1b, 1c, 1d
RS6-2-1	Ilmenite[a]	Plate-like, rough, complex	0.5–1 μm	1e, 1f
		Plate, branch-like	30–100 nm	2g
		Lens-like	~ 2–100 nm	2f, 2h
	Rutile[c]	Plate-like	50–200 nm	1e, 1f, 2f

[a] The very fine ilmenite lamellae with thickness <10 nm are approximately five times more in AD34-5 and AD34-4B than in RS6-2-1.
[b] Similar microstructures were observed in titanohematite grains of RS6-2-1.
[c] The plate-like rutile in RS6-2-1 is the different occurrence in AD34-5 and AD34-4B. See the text.

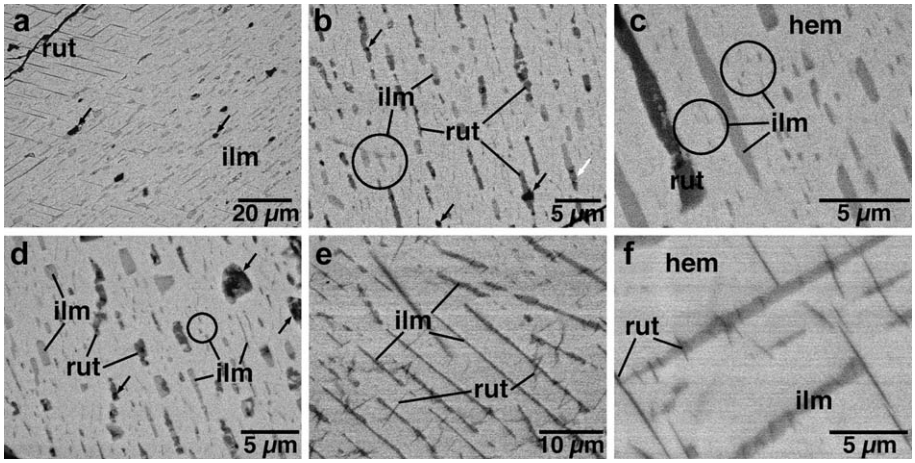

Fig. 1. Back-scattered electron images of titanohematite grains in AD34-5 (a, b, c), AD34-4B (d) and RS6-2-1 (e, f). (a) Ilmenite lamellae (center to right) and rutile lamellae (upper left) separated from one another within titanohematite grains. Precipitates indicated by black arrows are spinel. (b) Lens- and cylinder-like ilmenite (gray) and rutile (dark gray) lamellae in a titanohematite host (bright gray) that has mainly ilmenite lamellae. Precipitates indicated by black arrows are spinel. A white arrow shows rutile lamellae replaced partly by ilmenite. (c) Fine ilmenite lamellae, ~ 100 nm thick, between coarse lamellae. (d) Lens- and cylinder-like ilmenite (gray) and rutile (dark gray) lamellae in titanohematite. Precipitates with black contrast as indicated by black arrows are spinel. The texture of (d) is similar to that of (a). (e) Ilmenite lamellae (gray) with plate-like and rough, complex shapes in titanohematite (bright gray), and fine plate-like rutile lamellae (dark gray), which cut across the ilmenite lamellae. (f) Plate-like ilmenite lamellae with fine plate-like rutile lamellae. There are no fine lamellae between the coarse plate-like ilmenite lamellae. hem: titanohematite, ilm: ilmenite, rut: rutile.

c), and are partly replaced by ilmenite (a white arrow in Fig. 1b). The long-axes of the ilmenite and rutile lamellae in the titanohematite where ilmenite is predominantly present are preferentially oriented in the direction perpendicular to *c*-axis of titanohematite. The fine ilmenite lamellae observed between coarse lamellae are ~ 100 nm in thickness, which is equivalent to the smallest objects that are visible by SEM (Fig. 1c). The expectation that much finer ilmenite lamellae must exist in the titanohematite grains was confirmed by the present TEM study, described below. Although pyrophanite lamellae were found in all the samples, AD34-5 and AD34-4B have much smaller amounts of pyrophanite lamellae than RS6-2-1. The titanohematite grains in AD34-4B were quite similar to those in AD34-5 with respect to the morphologies and distributions of ilmenite and rutile lamellae (Fig. 1d).

Although titanohematite grains in RS6-2-1 have ilmenite and rutile lamellae, they are quite different from those in AD34-5 and AD34-4B. The rutile lamellae in RS6-2-1 are distributed throughout the titanohematite grains (Fig. 1e and f). The ilmenite lamellae in RS6-2-1 have mainly plate-like and rough, complex shapes and are oriented in different directions (Fig. 1e). Fine plate-like rutile lamellae cut across the ilmenite lamellae and are also present between the ilmenite lamellae (Fig. 1f). Fine ilmenite lamellae in RS6-2-1 are few in number compared with those in the titanohematite grains of AD34-5 and AD34-4B. Small titanohematite grains in AD34-5 and AD34-4B have similar textures to the dominant titanohematite grains in RS6-2-1, which also have few fine ilmenite lamellae. Hence, the small titanohematite grains where the fine rutile lamellae are present between the ilmenite lamellae and run across the ilmenite lamellae may inhibit the formation of fine ilmenite lamellae owing to Ti being consumed by the formation of rutile lamellae.

4.3. TEM observations of titanohematite grains with lamellae

TEM observations of titanohematite in AD34-5 indicated that very fine ilmenite lamellae are abundant between the ~ 100-nm ilmenite lamellae just observable by SEM (Figs. 1c and 2a). The very fine lamellae are surrounded by strain contrast that was produced by

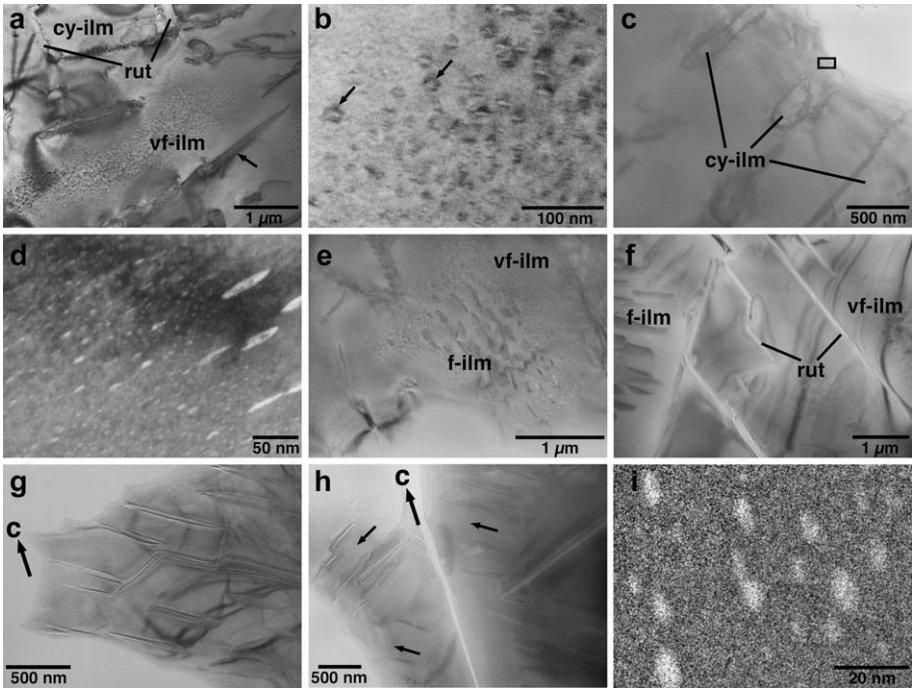

Fig. 2. TEM images of titanohematite grains in AD34-5 (a, b, c, d, i), AD34-4B (e) and RS6-2-1 (f, g, h). (a) Very fine ilmenite lamellae between coarse lamellae, and cylinder-like ilmenite lamella with rutile lamellae at its ends. The arrow indicates the ilmenite lamella deviated from the direction perpendicular to *c*-axis of its host, but such lamellae are rare. (b) Very fine ilmenite lamellae surrounded by strain contrast, which corresponds to darker contrast indicated by arrows. (c) Cylinder-like ilmenite lamellae with different sizes. Finer lamellae are absent between these lamellae. HRTEM image of a portion of the inset is shown in Fig. 3. (d) Dark-field image of very fine ilmenite lamellae in titanohematite hosts. This image was formed using the 003 reflection of ilmenite, so that ilmenite appears bright. (e) Very fine and fine ilmenite lamellae between coarse lamellae. The texture of (d) is similar to that of (a). (f) Plate-like rutile lamellae distributed like a net, and fine and very fine ilmenite lamellae between the rutile. (g) Fine branch-like ilmenite lamellae with $\sim$ 100 nm in thickness existing as a group. There are no finer ilmenite lamellae between them. The *c*-axes of the ilmenite lamellae and titanohematite are at an angle of 38° to the page. (h) Fine ilmenite lamellae showing two different orientations (arrows). Both lamellae share the same crystallographic axes with their hosts. The *c*-axes of the ilmenite lamellae are at an angle of 38° to the page. (i) Element map for Ti of very fine ilmenite lamellae in a titanohematite host. Titanium component is displayed as a bright region. cy-ilm: cylinder-like ilmenite lamellae, vf-ilm: very fine ilmenite lamellae with <20 nm in thickness, f-ilm: fine ilmenite lamellae with <100 nm in thickness, rut: rutile.

matching the two different lattice spacings of titanohematite and ilmenite (dark contrast in Fig. 2b), implying that they have a crystallographically coherent relationship with their hosts [23,24,32]. The long-axes of many ilmenite lamellae are preferentially oriented in the direction perpendicular to the *c*-axes of their hosts. The very fine lamellae tend to be formed when the distance between coarser lamellae is more than 1 μm (compare Fig. 2a and c). Dark-field (DF) images and selected-area electron diffraction patterns of very fine ilmenite lamellae revealed that the ilmenite lamellae <10 nm in thickness lie on (001) planes of the titanohematite hosts (Fig. 2d) and the boundaries between titanohematite with $R\bar{3}c$ symmetry and ilmenite with $R\bar{3}$ symmetry are structurally sharp, which are consistent with the presence of the boundaries with strain contrast. Similar DF images have been observed in igneous and metamorphic rocks [32,33], indicating that the exsolved lamellae of hematite and ilmenite commonly have a sharp structural interface with their hosts. Titanohematite grains in AD34-4B are quite similar to those in AD34-5 and possess abundant very fine ilmenite lamellae (Fig. 2e). The titanohematite grains in AD34-5 and AD34-4B also contain cylinder-like ilmenite lamellae with rutile lamellae at each end (Fig. 2a and c), which were also observed by SEM

(Fig. 1b–d). Titanohematite grains in RS6-2-1 have many long, plate-like rutile lamellae, which are distributed like a net even at the TEM level (Fig. 2f). The narrow spaces between the plate-like rutile lamellae have a few fine ilmenite lamellae. Plate, branch-like ilmenite lamellae with 100 nm thickness commonly exist and fine lamellae are absent in such an area (Fig. 2g). Although very fine lamellae were observed in the titanohematite grains of RS6-2-1 (Fig. 2f), they were present only in the spaces where the distance between the coarser lamellae (>100 nm in thickness) was greater than 1.5 μm. TEM observations of the very fine lamellae with thicknesses <10 nm in all the samples indicated that the very fine lamellae in AD34-5 and AD34-4B are at least five times as abundant as those in RS6-2-1. All the ilmenite lamellae observed in RS6-2-1 perfectly share the same crystallographic axes with their hosts, although the long-axes of many lamellae deviate by a few tens of degrees from the direction perpendicular to *c*-axes of their hosts (Fig. 2f–h). The features of major lamellae present in titanohematite grains are summarized in Table 4.

4.4. HRTEM observations of interfaces between titanohematite and ilmenite lamellae

Fig. 3 shows a HRTEM image of the cylinder-like ilmenite lamella with rutile lamellae on both the ends and a typical interface between the ilmenite lamellae

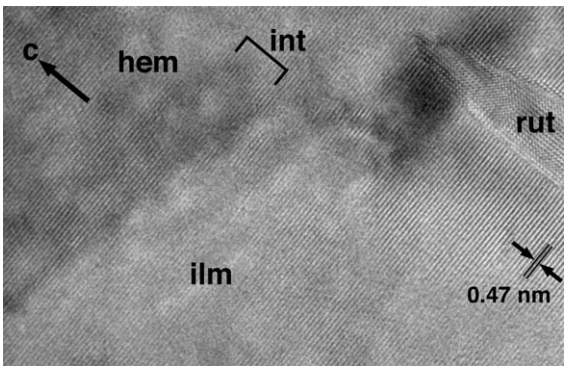

Fig. 3. HRTEM image of a cylinder-like ilmenite lamella, terminated by a rutile lamella, in a titanohematite host of AD34-5. This image is a portion of the inset in Fig. 2c. The beam direction for ilmenite and hematite is ⟨120⟩ and that for rutile ⟨001⟩. hem: titanohematite, ilm: ilmenite, rut: rutile, int: interface between titanohematite and ilmenite.

and their titanohematite hosts observed in AD34-5 and AD34-4B. The beam direction for ilmenite and hematite is ⟨120⟩ and that for rutile ⟨001⟩. Ilmenite and rutile contact at the ilmenite $\{2\bar{1}\ 0\}$ and rutile {100} planes. The HRTEM image indicated that ilmenite and titanohematite share (001) planes as expected from their crystallographic relationship, corresponding well to the previous HRTEM results [32], which were obtained from a hemo-ilmenite sample whose stable NRM has been controlled by lamellar magnetism [24]. The cylinder-like ilmenite lamellae are always terminated at both ends by rutile lamellae, which might be related to the morphology of the cylinder-like ilmenite lamellae since ilmenite lamellae without rutile at their ends usually take lens-like shapes [23,24,33].

4.5. Chemistry in titanohematite with lamellae and end-member hematite grains

McEnroe and Brown [21] have provided detailed electron probe microanalysis (EPMA) data on Russell Belt samples. Samples from sites AD34 and RS6 (including AD34-5 and AD34-4B and RS6-2-1, respectively) had large MD size hematite grains without exsolution with compositions of Hem_{98} to Hem_{100}, corresponding to end-member hematite in this study. The remaining 2% was made up of Ti, Al or Mn, substituting Fe^{3+} in the octahedral site. Titanohematite grains with lamellae had host compositions ranging from Hem_{72} to Hem_{86} (28–14% ilmenite component) and up to 1% as pyrophanite component. The parts of the ilmenite and pyrophanite components were likely due to overlap analyses of the host with fine ilmenite lamellae because the EPMA beam diameter is much larger than the size of the fine lamellae. Titanohematite grains contained abundant ilmenite lamellae (Ilm_{86-99}) which have small amounts of both pyrophanite and geikielite [$MgTiO_3$] components. Magnetite grains had nearly close to end-member composition with only 1wt% of TiO_2, Al_2O_3, or MnO. Because of the fine-scale of the exsolution lamellae, TEM-EDX analysis was necessary to obtain accurate compositions.

TEM–EDX analyses of the ilmenite lamellae and titanohematite host grains are shown in Table 5 and gave the following results: (i) lamellae and hosts of AD34-5=$Ilm_{93-100}Hem_{7-0}$ and $Ilm_{9-12}Hem_{91-88}$; (ii) lamellae and hosts of AD34-4B=$Ilm_{97-100}Hem_{3-0}$ and

$Ilm_{8-12}Hem_{92-88}$; (iii) lamellae and hosts of RS6-2-1=$Ilm_{90-100}Hem_{10-0}$ and $Ilm_{7-16}Hem_{93-84}$. Although $MnTiO_3$ content of the wide range of $<\sim 25\%$ was detected in the ilmenite lamellae, we regarded $MnTiO_3$ as part of the 'ilmenite' component when calculating the chemical composition of the ilmenite lamellae because $MnTiO_3$, i.e., pyrophanite has a space group of $R\bar{3}$ and a Néel temperature at -210 °C, thus similar crystallographically and magnetically to ilmenite (Table 2) [29,34]. The host titanohematite did not contain any detectable Mn. Thus, the chemical compositions between the three samples did not show any significant differences. TEM–EDX analyses did not indicate the presence of any other elements except those mentioned above in the ilmenite lamellae and titanohematite grains. In the end-member hematite grains, only Fe and O were detected (Table 5), consistent with the EPMA analyses of McEnroe and Brown [21].

Fig. 2i shows an element map for Ti of very fine ilmenite lamellae in the titanohematite of AD34-5 using EFTEM. AD34-4B and RS6-2-1 also showed similar element maps of very fine lamellae. The element maps, which revealed the presence of finer lamellae than those obtained by DF imaging, indicated that the very fine lamellae exist down to a minimum thickness of ~ 2 nm. Similar images also have been obtained in other metamorphic and igneous rocks with a stable, high NRM where these interfaces between hematite and ilmenite showed sharp compositional changes [23,24,31,32].

4.6. Microstructure of end-member hematite/magnetite grains in AD34-4B

Large end-member hematite grains in AD34-4B often have regions varying in reflectivity (Fig. 4). The EBSD and EDX analyses attached to SEM showed these grains are mainly made up of end-member magnetite with 20–150 μm in size together with the end-member hematite. XRD analyses found magnetite and hematite and a trace amount of maghemite. We could not confirm the presence of maghemite by LM or SEM with EDX because of the small amount and its similar composition to magnetite and hematite. Although end-member hematite is present in AD34-5 and RS6-2-1 (Table 3), in those cases, the end-member hematite is almost never accompanied by magnetite as shown in Fig. 4. The end-member hematite can contain precipitates of muscovite locally, however, their presence is extremely rare.

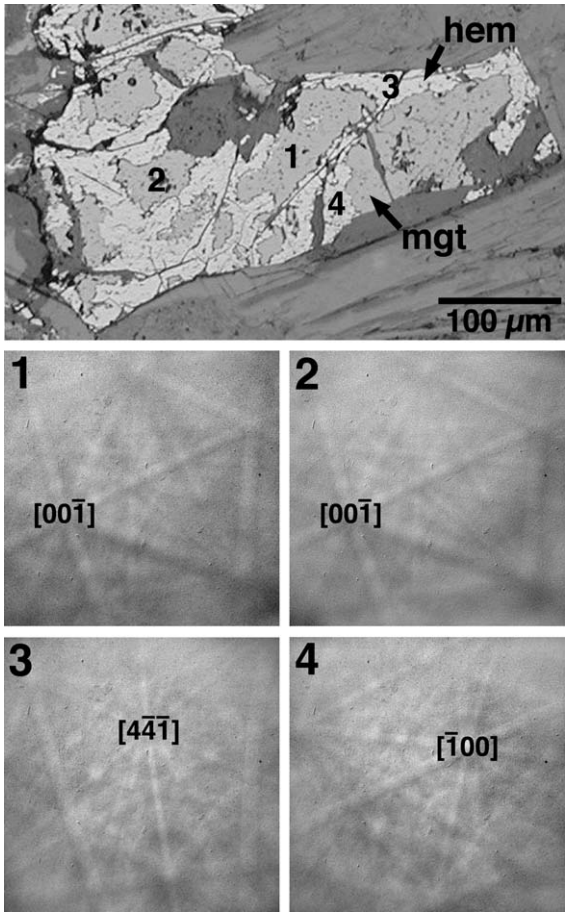

Fig. 4. Reflected-LM image and EBSD patterns of opaque minerals in AD34-4B. The numbers in the LM image indicate the area analyzed by EBSD and correspond to figures 1, 2, 3 and 4 of the EBSD patterns, respectively. The numbers in brackets are zone axes. hem: end-member hematite, mgt: magnetite.

4.7. Magnetic susceptibility

Temperature-dependent magnetic mass susceptibilities of the samples are shown in Fig. 5. The susceptibility curves of AD34-5 and RS6-2-1 are similar to one another and show very low susceptibilities, of $\sim 0.1 \times 10^{-6}$ m^3/kg from -190 to 600 °C (Fig. 5a and c). The peak near 130 °C in AD34-5 may be due to goethite, which is an alteration product of hematite (Fig. 5a). In AD34-5 and RS6-2-1, their susceptibilities

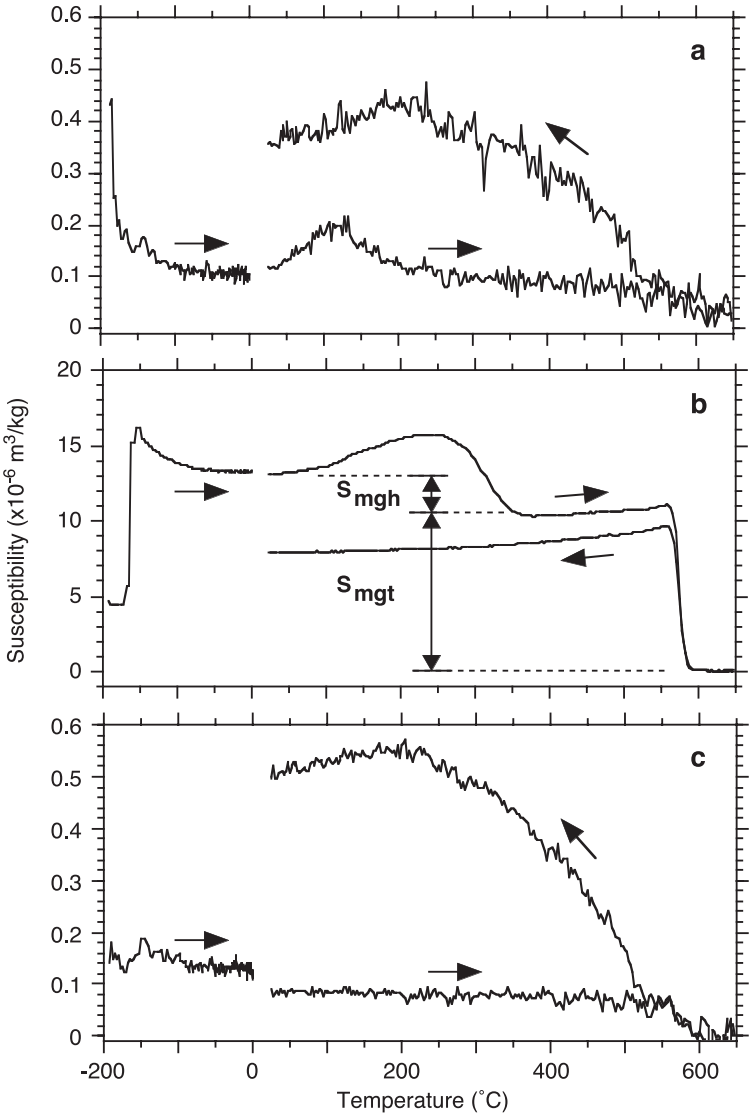

Fig. 5. Magnetic mass susceptibilities as a function of temperature for AD34-5 (a), AD34-4B (b) and RS6-2-1 (c). The S_{mgt} and S_{mgh} in (b) indicate intensities of susceptibilities caused by magnetite and maghemite, respectively.

are relatively constant until ~ 600 °C, apart from the peak at 130 °C in AD34-5, and are controlled by hematite and titanohematite.

In contrast, the susceptibility curve of AD34-4B has a higher value by two orders of magnitude than those of AD34-5 and RS6-2-1 (Fig. 5b) due to the presence of a small amount of MD size magnetite. The increase at ~ − 150 °C and decrease at ~ 580 °C corresponds to the Verwey transition and Curie temperature of magnetite, respectively. The initial rise in susceptibility with temperature up to ~ 250 °C is likely due to a small amount of maghemite that transformed between 250 and 300 °C to hematite (S_{mgh} in Fig. 5b). This is an inversion of γ-Fe_2O_3 to α-Fe_2O_3 and is an irreversible process. To check if this behavior was due to this chemical transition, the susceptibility measurement was repeated from room temperature to 300 °C. The second susceptibility run had lower values and only a

slight increase between room temperature to 300 °C. Comparison of the susceptibilities among the three samples suggests that AD34-4B contains rare magnetite and maghemite, consistent with the XRD data, while in AD34-5 and RS6-2-1, magnetite and maghemite are extremely rare.

4.8. Magnetic and hysteresis properties

A summary of the bulk magnetic properties as reported by McEnroe and Brown [21] is given below in addition to new rock magnetic data. All samples from the Russell Belt showed high thermal stability with little loss in magnetization by 600 °C, with medium destructive temperatures of ~630 °C or greater. The magnetic stability is also very high, with medium destructive fields well above 100 mT in alternating field demagnetization. Though room temperature hysteresis loops of the samples studied by TEM displayed two distinct types of behavior, all samples had symmetrical hysteresis loops about the origin indicating that exchange coupling is not important, however, this cannot be fully ruled out. Sample RS6-2-1 has restricted or ''wasp-waisted'' loops nearly identical to those shown by McEnroe and Brown [21] for other samples from this site. In addition, they made elevated temperature hysteresis measurements from room temperature to 700 °C on RS6-2-1 [21]. The room temperature loops showed the presence of three phases with a slight constriction near the origin and at the shoulders. Between 575 and 600 °C, the constriction at the origin is lost, and a lozenge-shaped loop is retained until 670 °C, suggesting that this sample contains titanohematite and hematite as SD to MD size grains, coupled with PSD or MD size magnetite. However, the amount of magnetite was interpreted to be very small because the loss in saturation magnetization between 575 and 600 °C was small.

In contrast, AD34-5 and AD34-4B have lozenge-shaped hysteresis loops with only a minor constriction at the shoulders of the loops. According to McEnroe and Brown [21], samples with this type of behavior contained titanohematite and hematite of effective SD and MD size grains, and typically no, or very rare magnetite. Samples showed values of coercivity of saturation (*Hc*) from 145 to 332 mT, more than 10 times the expected *Hc* values for MD hematite or MD magnetite. These measurements agree with the bulk magnetic properties of low susceptibility, high unblocking temperatures and medium destructive fields, indicating that magnetite is very rare. The two samples with the high NRMs also have higher saturation remanence (M_{rs}) and saturation magnetization (M_s) values by an order of magnitude than RS6-2-1 (Table 1). The M_{rs}/M_s values from 0.62 to 0.67, and the ratio of coercivity of remanence to saturation coercivity, H_{cr}/H_c values from 1.0 to 1.4 are similar for the three samples and are likely dominated by the exsolved titanohematite grains.

5. Discussion

5.1. Magnetite coexisting with end-member hematite

End-member hematite was observed in all the samples and locally can have end-member magnetite as inclusions. The LM observations, EBSD analyses and temperature-dependent magnetic susceptibility measurement indicated that AD34-4B had the most magnetite and maghemite in all the samples (Figs. 4 and 5b), suggesting that the higher susceptibility of AD34-4B (Table 1) measured by McEnroe and Brown [21] is due to magnetite coexisting with end-member hematite.

EBSD revealed that magnetite always has the same crystallographic orientation (e.g., the magnetite parts 1 and 2 in Fig. 4 have the same EBSD patterns). In contrast, end-member hematite has a random crystallographic orientation between neighboring grains (e.g., parts 3 and 4 in Fig. 4). It is observed in Fig. 4 that end-member hematite is also present along the cracks. These results suggest that the texture in the figure was formed by partial alteration of a large magnetite grain to hematite (i.e., martization) and maghemite by oxidative hydrothermal reaction as described by Buddington et al. [30]. The small amount of magnetite left in AD34-4B may result from a lower degree of alteration because the primary magnetite grain sizes in AD34-4B were larger than those in AD34-5 or RS6-2-1.

5.2. Contributors to acquisition of the NRM

Magnetite is one of the most common magnetic minerals in rocks, and small magnetite grains with

sizes 0.02 to a few micrometers have SD- to PSD-magnetic structures and can be a dominant carrier of remanent magnetization in rocks [6]. Larger magnetite grains with 20–200 μm sizes have appreciably lower remanent magnetizations, coercivities and thermal stabilities than the smaller magnetite grains because of their MD structures. Magnetite grains observed in this study have sizes in the range of 20–150 μm all in the MD range, indicating that magnetite is not a dominant carrier of the stable NRM in these rocks. Our results indicate that AD34-5, which has extremely rare magnetite and maghemite, had the highest NRM of the three samples, although AD34-4B, with rare magnetite and maghemite (Figs. 4 and 5b), also had a high NRM intensity (Table 1). Most of the Russell Belt samples retain 90% or more of the original NRM to 600 °C, well above the Curie temperature of magnetite [21]. Therefore, the NRM in these rocks does not depend on the presence of magnetite.

It is unlikely that pyrophanite is a carrier of NRM because it is paramagnetic at room temperature, although the detailed magnetic properties have not yet been determined [29,34]. McEnroe and Brown [21] suggested that the contribution of pyrophanite to the NRM in these samples may be only minor on the basis of the evidence that the samples with the most amount of pyrophanite had comparatively lower NRMs. Our LM and SEM observations agree with their interpretation.

When hematite–ilmenite solid solutions have composition ranging from $Ilm_{50-85}Hem_{50-15}$, they can act as ferrimagnets at low temperature and important carriers for NRM [2]. In all the samples, the composition ranges of the ilmenite lamellae were from $Ilm_{90-100}Hem_{10-0}$, and those of the titanohematite hosts from $Ilm_{7-16}Hem_{93-84}$. The compositions of the ilmenite lamellae and titanohematite hosts are out of the composition ranges where hematite–ilmenite solid solutions can have this strong ferrimagnetic intensity. In addition, the thermal stability of these samples is well above any compositions of ilmenite in the ferrimagnetic range [21], suggesting that the NRM acquisition by this mechanism has not occurred.

Coarse hematite grains with MD structures can acquire intense TRM if obtained just below the blocking temperature. Since end-member hematite grains observed in this study have mostly grain sizes of >50 μm (Table 3), which correspond to MD hematite sizes, end-member hematite should be a significant contributor to the NRM. However, AD34-5 has a considerably stronger NRM than RS6-2-1, which our observations have shown to contain twice the amount of end-member hematite. The Russell Belt samples have high coercivities, and only a small percent of the NRM remaining above 650 °C, a temperature below the Néel temperature of the unexsolved MD size hematite grains close to the end-member composition with <2% atomic percentage Al or Ti [21]. We conclude that MD size hematite in these samples is not a major contributor to acquisition of the magnetization.

Monte Carlo simulations have predicted that the ferrimagnetic moment could occur at the interface of hematite and ilmenite, a phenomenon termed ‘‘lamellar magnetism’’ [25–27]. Kasama et al. [32] showed by HRTEM and EFTEM that hematite and ilmenite have coherent, sharp structural and compositional interfaces, consistent with the predictions of Monte Carlo simulations of the exsolution process. The present TEM observations also show similar microstructures of ilmenite lamellae ($Ilm_{90-100}Hem_{10-0}$) and titanohematite hosts ($Ilm_{7-16}Hem_{93-84}$), sharing (001) planes and containing abundant fine ilmenite lamellae with coherent, sharp structural and compositional interfaces with their titanohematite hosts (Table 5; Figs. 2 and 3).

5.3. Relationships between fine lamellae and magnetization

The carrier of the NRM in the Russell Belt samples is most likely related to the finely exsolved ilmenite lamellae observed in the titanohematite grains in all three samples. However, although the lamellar magnetism hypothesis is predicted by Monte Carlo simulations [25,26] and a few studies have attributed stable NRMs to the presence of such fine lamellae [23,24,27], the hypothesis has not been proved completely by observations and experiments. Samples AD34-5 and RS6-2-1 experienced the same geological history. Although both samples have magnetite and MD size hematite, these minerals are minor contributors to magnetic acquisition in this study. Hence, AD34-5 and RS6-2-1 are ideal samples to examine the effects of finely exsolved lamellae on acquiring magnetization. We will discuss the validity

Table 5
TEM–EDX analyses of the titanohematite hosts, ilmenite lamellae and end-member hematite in each sample

Sample	Analyzed area	Calculated percentage of the end-members[a]			Ilmenite and hematite components[b]
		Fe_2O_3	$FeTiO_3$	$MnTiO_3$	
AD34-5	Lamella 1	0	91	9	$Ilm_{100}Hem_0$
	Lamella 2	0	94	6	$Ilm_{100}Hem_0$
	Lamella 3	2	95	3	$Ilm_{98}Hem_2$
	Lamella 4	4	89	7	$Ilm_{96}Hem_4$
	Lamella 5	7	90	3	$Ilm_{93}Hem_7$
	Host 1	88	12	n.d.	$Ilm_{12}Hem_{88}$
	Host 2	89	11	n.d.	$Ilm_{11}Hem_{89}$
	Host 3	89	11	n.d.	$Ilm_{11}Hem_{89}$
	Host 4	90	10	n.d.	$Ilm_{10}Hem_{90}$
	Host 5	92	8	n.d.	Ilm_8Hem_{92}
	Hematite[c] 1	100	n.d.	n.d.	Ilm_0Hem_{100}
	Hematite[c] 2	100	n.d.	n.d.	Ilm_0Hem_{100}
	Hematite[c] 3	100	n.d.	n.d.	Ilm_0Hem_{100}
AD34-4B	Lamella 1	0	89	11	$Ilm_{100}Hem_0$
	Lamella 2	1	91	8	$Ilm_{99}Hem_1$
	Lamella 3	1	77	22	$Ilm_{99}Hem_1$
	Lamella 4	2	76	22	$Ilm_{98}Hem_2$
	Lamella 5	3	79	18	$Ilm_{97}Hem_3$
	Host 1	88	12	n.d.	$Ilm_{12}Hem_{88}$
	Host 2	88	12	n.d.	$Ilm_{12}Hem_{88}$
	Host 3	89	11	n.d.	$Ilm_{11}Hem_{89}$
	Host 4	89	11	n.d.	$Ilm_{11}Hem_{89}$
	Host 5	91	9	n.d.	Ilm_9Hem_{91}
	Hematite[c] 1	100	n.d.	n.d.	Ilm_0Hem_{100}
	Hematite[c] 2	100	n.d.	n.d.	Ilm_0Hem_{100}
	Hematite[c] 3	100	n.d.	n.d.	Ilm_0Hem_{100}
RS6-2-1	Lamella 1	0	90	10	$Ilm_{100}Hem_0$
	Lamella 2	0	90	10	$Ilm_{100}Hem_0$
	Lamella 3	4	87	9	$Ilm_{96}Hem_4$
	Lamella 4	9	68	23	$Ilm_{91}Hem_9$
	Lamella 5	10	68	22	$Ilm_{90}Hem_{10}$
	Host 1	84	16	n.d.	$Ilm_{16}Hem_{84}$
	Host 2	88	12	n.d.	$Ilm_{12}Hem_{88}$
	Host 3	90	10	n.d.	$Ilm_{10}Hem_{90}$
	Host 4	92	8	n.d.	Ilm_8Hem_{92}
	Host 5	93	7	n.d.	Ilm_7Hem_{93}
	Hematite[c] 1	100	n.d.	n.d.	Ilm_0Hem_{100}
	Hematite[c] 2	100	n.d.	n.d.	Ilm_0Hem_{100}
	Hematite[c] 3	100	n.d.	n.d.	Ilm_0Hem_{100}

n.d. = not detected by TEM–EDX.
[a] Any other elements except Fe, Ti, Mn or O were not detected by TEM–EDX.
[b] $MnTiO_3$ was regarded as part of the 'ilmenite' component when calculating the chemical composition of the ilmenite lamellae.
[c] Hematite is equal to end-member hematite in the text.

of the lamellar magnetism hypothesis by comparing the two samples.

Robinson et al. [26] described some conditions necessary to obtain a strong magnetization by lamellar magnetism: (1) the proportion of exsolved lamellar material is large, (2) lamellae are abundantly present with a fine size and (3) the (001) planes of hosts are parallel to the magnetic field. Conditions (1) and (2) are related to the surface area of interfaces between hematite and ilmenite produced by lamellae. Condition (3) means that the magnetic field parallel to (001) planes allows the ferrimagnetic moment

occurring at the interface to orient easily in a direction parallel to the magnetic field. The small difference of the inclination and declination of NRM between AD34-5 and RS6-2-1 means little effect of condition (3) on the difference of their NRM intensities (Table 1).

Our LM and TEM observations revealed that AD34-5 has about five times more titanohematite grains with lamellae than RS6-2-1 (Table 3), and approximately five times the number of very fine ilmenite lamellae than RS6-2-1 (Table 4; Fig. 2). Although, in RS6-2-1, the orientation of the long-axes of the ilmenite lamellae deviated by up to a few tens of degrees from an orientation perpendicular to the *c*-axes of their hosts, its effect on the intensity of lamellar magnetization is small because the crystallographic orientations between lamellae and hosts are perfect, as they share (001) planes. The chemical composition of the ilmenite lamellae and titanohematite hosts may also be associated with an intensity of magnetization but this effect may be ignored because the chemical compositions of the two samples are similar to one another and out of the composition ranges where hematite–ilmenite solid solutions can have strong ferrimagnetic intensities (Table 5).

Our observations suggest that AD34-5 could have roughly 25 times stronger magnetization than RS6-2-1, while the NRM intensity of AD34-5, at 8.45 A/m, is about 60 times stronger than that of RS6-2-1 at 0.15 A/m. An order of magnitude difference between the NRMs of the two samples can be explained by the amount of material with finely exsolved ilmenite lamellae in the titanohematite. These results strongly support lamellar magnetization as a reasonable model, and a likely mechanism for NRM acquisition in the Russell Belt. Since lower crustal rocks can contain hematite and ilmenite lamellae exsolved during slow cooling [35], magnetic acquisition by lamellae formation may be a predominant mechanism in the crust, as has been previously suggested by McEnroe et al. [21,23,24].

Acknowledgements

We thank P. Robinson of Geological Survey of Norway for comments on an earlier version of this manuscript, A. Hirt of Swiss Federal Institute of Technology (ETH) for providing the hysteresis measurements and O. Tachikawa of The University of Tokyo for SEM observations. This manuscript was greatly improved by L. Brown, D. Dunlop and an anonymous reviewer. This work is supported by the Deutsche Forschungsgemeinschaft (Grant PU 153/2-3). ***[BW]***

References

[1] T. Nagata, S. Uyeda, S. Akimoto, Self-reversal of thermoremanent magnetization of igneous rocks, J. Geomagn. Geoelectr. 4 (1952) 22–38.
[2] G.L. Nord Jr., C.A. Lawson, Order–disorder transition-induced twin domains and magnetic properties in ilmenite–hematite, Am. Mineral. 74 (1989) 160–176.
[3] R.J. Harrison, A. Putnis, The magnetic properties and crystal chemistry of oxide spinel solid solutions, Surv. Geophys. 19 (1999) 461–520.
[4] G.D. Price, Exsolution microstructures in titanomagnetites and their magnetic significance, Phys. Earth Planet. Inter. 23 (1980) 2–12.
[5] J.F. Banfield, P.J. Wasilewski, D.R. Veblen, TEM study of relationships between the microstructures and magnetic properties of strongly magnetized magnetite and maghemite, Am. Mineral. 79 (1994) 654–667.
[6] D. Dunlop, Ö. Özdemir, Rock Magnetism: Fundamentals and Frontiers, Cambridge Univ. Press, Cambridge, 1997573 pp.
[7] Y. Ishikawa, S. Akimoto, Magnetic properties of the $FeTiO_3$–Fe_2O_3 solid solution series, J. Phys. Soc. Jpn. 12 (1957) 1083–1098.
[8] Y. Ishikawa, Magnetic properties of ilmenite–hematite system at low temperature, J. Phys. Soc. Jpn. 17 (1962) 1835–1844.
[9] K.A. Hoffman, Self-reversal of thermoremanent magnetization in the ilmenite–hematite system: order–disorder, symmetry, and spin alignment, J. Geophys. Res. 97 (1992) 10883–10895.
[10] M. Prévot, K.A. Hoffman, A. Goguitchaichvili, J.-C. Doukhan, V. Shcherbakov, M. Bina, The mechanism of self-reversal of the thermoremanence in natural hemoilmenite crystals: new experimental data and model, Phys. Earth Planet. Inter. 126 (2001) 75–92.
[11] Y. Syono, S. Akimoto, T. Nagata, Remanent magnetization of ferromagnetic single crystal, J. Geomagn, Geoelectr. 14 (1962) 113–124.
[12] S. Uyeda, Thermo-remanent magnetism as a medium of paleomagnetism, with special reference to reverse thermo-remanent magnetism, Jpn. J. Geophys. 2 (1958) 1–123.
[13] D.A. Clark, Magnetic petrophysics and magnetic petrology: aids to geologic interpretation of magnetic surveys, J. Aust. Geo. Geophys. 17 (1997) 83–103.
[14] D.J. Dunlop, G. Kletetschka, Multidomain hematite; a source of planetary magnetic anomalies? Geophy. Res. Lett. 28 (2001) 3345–3348.

[15] J.R. Balsely, A.F. Buddington, Correlation of reversed remanent magnetism and negative anomalies with certain minerals, J. Geomagn. Geoelectr. 6 (1954) 176–181.
[16] J.R. Balsely, A.F. Buddington, Iron–titanium oxide minerals, rocks, and aeromagnetic anomalies of the Adirondack area, New York, Econ. Geol. 53 (1958) 777–895.
[17] R.B. Hargraves, Magnetic anisotropy and remanent magnetization in hemo-ilmenite from ore deposits of Allared Lake, Quebec, J. Geophys. Res. 64 (1959) 1565–1573.
[18] C.M. Carmichael, Remanent magnetism of the Allard Lake ilmenite, Nature 183 (1959) 1239–1241.
[19] C.M. Carmichael, The magnetic properties of ilmenite–hematite crystals, Proc. R. Soc. Lond., Ser. A 263 (1961) 508–530.
[20] S.A. McEnroe, Ilmenite mineral magnetism: implications for geophysical exploration for ilmenite deposits, Nor. Geol. Surv. Bull. 433, (1997) 36–37.
[21] S.A. McEnroe, L.L. Brown, A closer look at remanence-dominated aeromagnetic anomalies: rock magnetic properties and magnetic mineralogy of the Russell Belt microcline-sillimanite gneiss, northwest Adirondack Mountains, New York, J. Geophys. Res. 105 (2000) 16437–16456.
[22] S.A. McEnroe, P. Robinson, P. Panish, Aeromagnetic anomalies, magnetic petrology, and rock magnetism of hemo-ilmenite- and magnetite-rich cumulate rocks from the Sokndal Region, South Rogaland, Norway, Am. Mineral. 86 (2001) 1447–1468.
[23] S.A. McEnroe, R.J. Harrison, P. Robinson, U. Golla, M.J. Jercinovic, Effect of fine-scale microstructures in titanohematite on the acquisition and stability of natural remanent magnetization in granulite facies metamorphic rocks, southwest Sweden: implications for crustal magnetism, J. Geophys. Res. 106 (2001) 30523–30546.
[24] S.A. McEnroe, R.J. Harrison, P. Robinson, F. Langenhorst, Nanoscale hematite–ilmenite lamellae in massive ilmenite rock: an example of "lamellar magnetism" with implications for planetary magnetic anomalies, Geophys. J. Int. 151 (2002) 890–912.
[25] R.J. Harrison, U. Becker, Magnetic ordering in solid solution, in: C.A. Geiger (Ed.), Solid Solutions in Silicate and Oxide Systems, EMU Notes Miner. 3. Eötvös Univ. Press, Budapest, 2001, pp. 349–383.
[26] P. Robinson, R.J. Harrison, S.A. McEnroe, R.B. Hargraves, Lamellar magnetism in the hematite–ilmenite series as an explanation for strong remanent magnetization, Nature 418 (2002) 517–520.
[27] P. Robinson, R.J. Harrison, S.A. McEnroe, R.B. Hargraves, The nature and origin of lamellar magnetism in the hematite–ilmenite series, Am. Mineral. 89 (2004) 725–747.
[28] R.T. Merrill, A possible source for the coercivity of ilmenite–hematite minerals, J. Geomagn. Geoelectr. 20 (1968) 181–185.
[29] H. Aruga-Katori, A. Ito, Magnetic property and phase diagram of a frustrated system with competing exchange interactions, $Fe_xMn_{1-x}TiO_3$, J. Phys. Soc. Jpn. 62 (1993) 4488–4502.
[30] A.F. Buddington, J. Fahey, A. Vlisidis, Degree of oxidation of Adirondack iron oxide and iron–titanium minerals in relation to petrogeny, J. Petrol. 4 (1963) 138–169.
[31] U. Golla, A. Putnis, Valence state mapping and quantitative electron spectroscopic imaging of exsolution in titanohematite by energy-filtered TEM, Phys. Chem. Miner. 28 (2001) 119–129.
[32] T. Kasama, U. Golla-Schindler, A. Putnis, High-resolution and energy-filtered TEM of the interface between hematite and ilmenite exsolution lamellae: relevance to the origin of lamellar magnetism, Am. Mineral. 88 (2003) 1190–1196.
[33] C.M. Schlinger, D.R. Veblen, Magnetism and transmission electron microscopy of Fe–Ti oxides and pyroxenes in a granulite from Lofoten, Norway, J. Geophys. Res. 94 (1989) 14009–14026.
[34] Y. Ishikawa, S. Akimoto, Magnetic property and crystal chemistry of ilmenite ($MeTiO_3$) and hematite (αFe_2O_3) system: II. Magnetic property, J. Phys. Soc. Jpn. 13 (1958) 1298–1310.
[35] B.R. Frost, D.H. Lindsley, Occurrence of iron–titanium oxides in igneous rocks, in: D.H. Lindsley (Ed.), Oxide Minerals: Petrologic and Magnetic Significance, Rev. Mineral. 25,Min-Mineral. Soc. of Am., Washington, DC, 1991, pp. 433–468.